Intracardiac Flow at 4D CT: Comparison with 4D Flow MRI

Jonas Lantz, PhD • Vikas Gupta, PhD • Lilian Henriksson, MSc • Matts Karlsson, PhD • Anders Persson, PhD, MD • Carl-Johan Carlhäll, PhD, MD • Tino Ebbers, PhD

From the Division of Cardiovascular Medicine, Department of Medical and Health Sciences (J.L., V.G., T.E.), Center for Medical Image Science and Visualization (CMIV) (J.L., V.G., L.H., M.K., A.P., C.J.C., T.E.), Division of Radiology, Department of Medical and Health Sciences (L.H., A.P.), Division of Applied Thermodynamics and Fluid Mechanics, Department of Management and Engineering (M.K.), and Department of Clinical Physiology, Department of Medical and Health Sciences (C.J.C.), Linköping University, SE-58183 Linköping, Sweden. From the 2017 RSNA Annual Meeting. Received January 16, 2018; revision requested March 5; final revision received April 27; accepted May 1. **Address correspondence to** J.L. (e-mail: *jonas.lantz@liu.se*).

The authors acknowledge funding from the Knut and Alice Wallenberg Foundation through the project *Seeing Organ Function* and from the Swedish Heart Lung Foundation. The Swedish National Infrastructure for Computing was acknowledged for computational resources provided by the National Supercomputer Centre (grant no. SNIC2014-11-22).

Conflicts of interest are listed at the end of this article.

See also the editorial by Schoepf and Varga-Szemes in this issue.

Radiology 2018; 00:1–8 • https://doi.org/10.1148/radiol.2018173017 • Content codes: CA CT MR

Purpose: To investigate four-dimensional (4D) flow CT for the assessment of intracardiac blood flow patterns as compared with 4D flow MRI.

Materials and Methods: This prospective study acquired coronary CT angiography and 4D flow MRI data between February and December 2016 in a cohort of 12 participants (age range, 36–74 years; mean age, 57 years; seven men [age range, 36–74 years; mean age, 57 years] and five women [age range, 52–73 years; mean age, 64 years]). Flow simulations based solely on CT-derived cardiac anatomy were assessed together with 4D flow MRI measurements. Flow patterns, flow rates, stroke volume, kinetic energy, and flow components were quantified for both techniques and were compared by using linear regression.

Results: Cardiac flow patterns obtained by using 4D flow CT were qualitatively similar to 4D flow MRI measurements, as graded by three independent observers. The Cohen κ score was used to assess intraobserver variability (0.83, 0.79, and 0.70) and a paired Wilcoxon rank-sum test showed no significant change ($P > .05$) between gradings. Peak flow rate and stroke volumes between 4D flow MRI measurements and 4D flow CT measurements had high correlation ($r = 0.98$ and $r = 0.81$, respectively; $P < .05$ for both). Integrated kinetic energy quantified at peak systole correlated well ($r = 0.95$, $P < .05$), while kinetic energy levels at early and late filling showed no correlation. Flow component analysis showed high correlation for the direct and residual components, respectively ($r = 0.93$, $P < .05$ and $r = 0.87$, $P < .05$), while the retained and delayed components showed no correlation.

Conclusion: Four-dimensional flow CT produced qualitatively and quantitatively similar intracardiac blood flow patterns compared with the current reference standard, four-dimensional flow MRI.

Online supplemental material is available for this article.

Cardiovascular hemodynamics play an important role in the initiation and progression of cardiovascular diseases. Recently, approaches have been developed for the assessment of cardiovascular blood flow dynamics (1,2). While some of these techniques are based on direct measurement of the flow field, others combine measurement with modeling approaches, all of which have different strengths and weaknesses. Noninvasive measurement of intracardiac blood flow dynamics is mostly performed by using phase-contrast MRI (four-dimensional [4D] flow MRI) or US. Complementary to measurements, simulations of blood flow by computational fluid dynamics are making their way into the clinic, most noticeably through the estimation of fractional flow reserve in the coronary arteries (3–6).

Cardiac blood flow patterns can also be simulated by using anatomic information obtained from CT (2) (hereafter referred to as 4D flow CT). With the aid of such modeling techniques, additional clinical information can potentially be extracted from a conventional CT scan. Recent studies (7,8) have shown that the intracardiac flow field strongly interacts with the endocardial surface, highlighting the need for well-resolved, patient-specific geometries. Several studies have investigated intracardiac blood flow using flow modeling (2,7–10), but these studies have not included a comprehensive quantitative comparison with three-dimensional time-resolved in vivo measurements.

We hypothesized that intracardiac blood flow information can be extracted from clinical coronary CT angiography acquisitions. To that end, we compared intracardiac blood flow in patients with heart disease using state-of-the-art 4D flow MRI and 4D flow CT to investigate the agreement and robustness of the 4D flow CT technique.

Materials and Methods

Participant Population

Between February and December 2016, 13 study participants who had a clinical referral for coronary CT angiography were enrolled in our prospective study, which was approved by the local ethics review board. Written

Abbreviations

4D = four-dimensional, LA = left atrium, LV = left ventricle

Summary

The proposed four-dimensional (4D) CT flow method produced similar intracardiac blood flow patterns to the current reference standard, 4D flow MRI.

Implications for Patient Care

- Clinical CT acquisitions enable the assessment of intracardiac flow patterns and kinetic energy levels, which are potential markers of cardiac function.
- Four-dimensional (4D) flow CT showed good qualitative and quantitative agreement with 4D flow MRI for the assessment of intracardiac flow patterns.

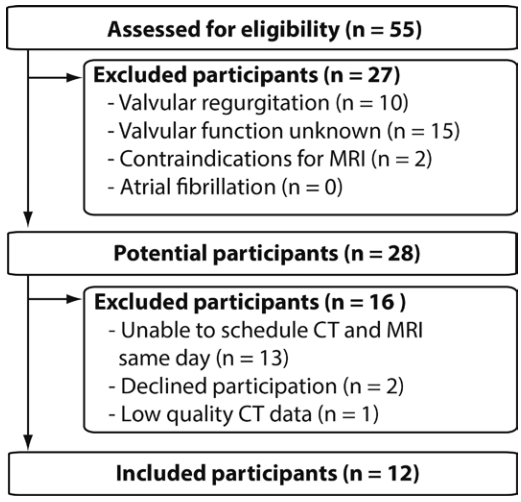

Figure 1: Flowchart shows recruitment of participants, along with inclusion and exclusion criteria.

informed consent was obtained from all participants. The participants underwent an MRI examination after the CT acquisition. The MRI acquisition was usually performed within 2 hours of the CT acquisition. Two participants had their MRI acquisition within a week after CT acquisition because of scheduling issues. Inclusion criteria were as follows: *(a)* successful coronary CT angiography acquisition, *(b)* no contraindications to MRI, *(c)* no atrial fibrillation, and *(d)* less than mild valvular regurgitation (based on earlier Doppler echocardiography data). One participant was excluded because of noisy CT data that introduced problems in wall-tracking processing. This was probably due to a too-low energy level (70 kV) given the participant's body mass index (29 kg/m^2) in combination with a metal cerclage that resulted in high image noise. Twelve participants were included in our final analysis (Fig 1, Table 1).

CT Acquisition

CT was performed by using a third-generation dual-source CT scanner (Somatom Force; Siemens Medical Solutions, Forchheim, Germany). Acquisition parameters are presented in Table 2. Retrospective image acquisition with electrocardiographically triggered dose modulation was used to cover the whole cardiac cycle. Following clinical protocol, data were acquired during inspiration breath holds. Multiphase image reconstructions were generated, including phases at every 5% between two R-R intervals from 0% to 95% (20 phases). The reconstructed section thickness was 0.5 mm with a 0.25-mm increment, and in-plane resolution was 0.353 × 0.353 mm ± 0.035. The mean radiation dose was 5.39 mSv and was computed according to European guidelines for multisection CT (11). β-Blockers were given to four participants to lower and stabilize the heart rate (see Table 1).

As previously described (8), intracardiac flow fields were computed based on acquired CT data (for details, see Appendix E1 [online]). An image registration framework developed by using Elastix (12) tracked the endocardial wall motion over the cardiac cycle. The extracted wall motion has been validated against manually segmented geometries, and, despite differences in image quality caused by dose modulation, contrast variation, and heterogeneous anatomy across multiple cardiac phases and participants, the tracking algorithm was shown to provide consistently high accuracy (13). Deformed cardiac geometries were generated every 10 msec for the entire cardiac cycle, and the flow field was computed by using the general-purpose computational fluid dynamics code CFX 17.0 (Ansys, Canonsburg, Pennsylvania). The temporal resolution of the simulations was 500 μsec. On the basis of the size of the heart, spatial resolution was in the range of 8–18 million computational cells, with the smallest length scale on the order of 50 μm to resolve high-curvature regions. Simulation time depended on heart size but was approximately 6–10 hours per cardiac cycle using 96 CPU cores.

MRI Acquisition

The MRI examination was performed by using a clinical 3.0-T Ingenia MRI unit (Philips Healthcare, Best, the Netherlands). The 4D flow data were acquired during free breathing by using a gradient-echo pulse sequence with interleaved three-directional flow encoding and retrospective vector cardiogram-controlled cardiac gating and respiratory navigator gating at end expiration. Imaging parameters are presented in Table 2. The acquired spatial resolution was 2.9 × 2.9 × 2.9 mm, with an effective acquired temporal resolution of 40 msec.

Evaluation

Similarities between MRI- and CT-derived flow patterns were assessed at peak systole and early diastolic filling in a three-chamber view independently by three observers (with 10, 4, and 2 years of experience in assessing cardiovascular flows). Flow patterns were visualized by using color-coded velocity magnitude and velocity vectors. The left atrium (LA) and left ventricle (LV) were assessed separately, similarity was graded from 0 (no similarity at all) to 4 (perfect similarity) (see Table E1 [online]), and median results were presented. Aortic and mitral flow rates and stroke volumes, as well as intracardiac kinetic energy, were extracted by using the open-source software Paraview (v5.4, Kitware, Clifton Park, NY). As previously described (14,15), flow component analyses characterizing the

Table 1: Participant Characteristics

Participant No.	Sex	Age (y)*	Heart Rate at CT (beats/min)	Heart Rate at MRI (beats/min)	Time between CT and MRI	LVEDV (mL)	LVESV (mL)	LVEF (%)	β-Blocker Use during CT
1	M	49	75	70	<2 h	145	76	47	Yes
2	F	52	79	73	<2 h	117	50	57	Yes
3	M	52	60	59	<2 h	120	46	62	No
4	F	66	66	65	<2 h	113	51	54	No
5	M	36	60	62	<2 h	248	164	34	No
6	M	57	63	63	1 week	100	38	62	Yes
7	M	74	77	74	<2 h	110	27	76	No
8	F	62	60	58	<2 h	94	42	56	No
9	F	73	59	58	<2 h	107	49	54	Yes
10	F	66	48	44	<2 h	106	60	43	No
11	F	47	57	55	1 week	170	89	48	No
12	F	46	54	37	<2 h	173	89	49	No

Note.—LVEDV = left ventricular end-diastolic volume, LVEF = left ventricular ejection fraction (derived from CT acquisition), LVESV = left ventricular end-systolic volume.

* Mean age for the entire cohort was 57 years (range, 36–74 years), while mean age for men was 52 years (range, 36–74 years), and mean age for women was 64 years (range, 52–73 years).

Table 2: Parameters for CT and MRI Acquisitions

Parameter	Value
CT	
Detector collimation (mm)	192 × 0.6
Gantry rotation time (sec)	0.25
Pitch	0.15–0.34
Quality reference (mAs)	276
Reference tube voltage (kV)	100
MRI	
Velocity encoding (cm/sec)	120
Flip angle (degrees)	5
Echo time (msec)	2.9
Repetition time (msec)	5.0
k-Space segmentation factor	2

multidimensional blood flow organization within the beating LV were computed for both CT and MRI. Pathlines were computed by using Ensight 10.2 (Ansys, Canonsburg, Pa) and were analyzed by using Matlab (R2016, Natick, Mass). By using this analysis, the path taken by the blood flow through the LV can be divided into the following four components: direct flow (which enters the LV and exits into the aorta in one heartbeat), retained inflow (which enters and resides in the LV for at least one heartbeat), delayed ejection flow (which resides inside the LV and exits during systole), and residual volume (which represents the blood volume that resides within the LV for at least two cardiac cycles). Internal assessment of MRI data quality was performed by visual inspection of these path lines and by checking the mitral inflow volume against the aortic outflow volume. In addition, because LV inflow equals direct flow plus retained inflow, and LV outflow equals direct flow plus delayed ejection flow, it follows by conservation of mass that the retained inflow and delayed ejection flow components should be equal. Flow component analysis can be sensitive to data artifacts and participant motion between acquisition of morphology and flow data. A ventricular inflow-outflow difference larger than 10% would render exclusion from the analysis (16).

Statistical Analysis

Grading of flow field similarity was performed independently by three observers two times with 12 weeks apart. The Cohen κ coefficient was calculated to assess intraobserver agreement. To determine if the second grading led to a significant change, a paired Wilcoxon rank-sum test was used.

Linear regression was used to analyze the correlation and agreement between the results from MRI and those from CT. MRI results were considered to be the independent variable, and flow rates, stroke volumes, intracardiac kinetic energy, and flow components were assessed. To assess agreement, coefficients for slope and intercept (and their respective *t* tests that the intercept coefficient was significantly different from 0 and the slope coefficient was significantly different from 1) were computed with 95% confidence intervals. Errors were assessed by using standard errors, and mean differences in parameter values from the two modalities were evaluated. Correlations were classified as strong ($r > 0.85$), good ($r = 0.70$–0.85), or fair ($0.50 < r < 0.70$). $P < .05$ was considered to indicate a statistically significant result. All statistical tests were performed by using Matlab 2016 (MathWorks, Natick, Mass).

Results

Flow Features Inside the Heart

The agreement in intracardiac flow patterns at peak systole (Fig 2 and Fig E1 [online]) and early filling (Fig E2 [online]) were qualitatively assessed by three observers. The Cohen κ scores for intraobserver agreement were 0.83, 0.79 and 0.70 for the three observers, and all discrepancies were within one grade level. The paired Wilcoxon rank-sum test showed no signifi-

cant difference in grade between first and second grading ($P > .05$). The median similarity of peak systolic flow patterns was graded at 2 for the LA and at 3 for the LV. The median similarity of early diastolic flow patterns was graded at 3 for both the LA and the LV.

For both modalities, at peak systole, the velocity was elevated in the LV outflow tract (LVOT) and ascending aorta as the blood was ejected through the aortic valve. For most participants, the ventricular systolic contraction increased the velocity in the entire ventricle, but, for larger LVs (eg, those in participants 4 and 5), most of the increase in velocity was seen close to the LVOT and septal wall. During early filling, the mitral valve directed the flow either toward the center of the ventricle (eg, in participants 1, 3, and 5) or toward the inferolateral wall, where it impinged on the myocardium (eg, in participants 4 and 7). The characteristic vortex that forms at the mitral leaflet tips was observed, and, for some participants (eg, participants 4 and 5), a large vortex formed in the center of the ventricle, which is common for dilated ventricles. Diastolic flow patterns were different between the participants, highlighting the heterogeneity of the participant cohort. However, on a per-participant basis, there were only minor differences between 4D flow MRI and 4D flow CT.

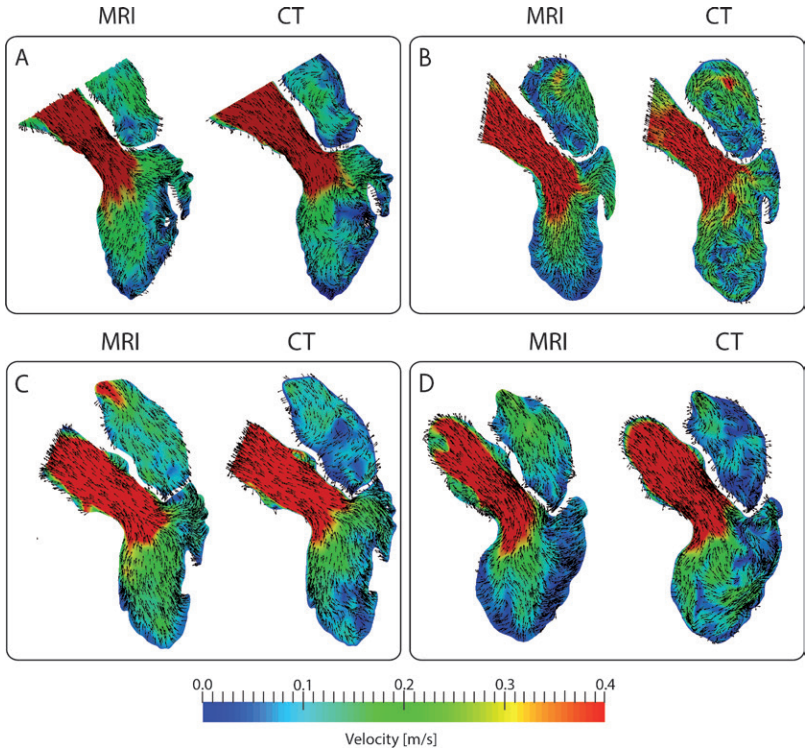

Figure 2: *A–D,* Quantitative comparison between four-dimensional flow and CT simulations for four of the 12 participants (participants 1–4 in *A–D,* respectively). Velocity magnitude and in-plane velocity vectors are shown in a three-chamber plane covering the atrium, ventricle, and ascending aorta at peak systole. (Results for all 12 participants can be found in Figure E1 [online].)

Valvular Flow and Stroke Volume

The LV outflow rates during systole showed minor differences between the methods (see Fig 3 and Fig E3 [online]). The upslope and peak of the aortic flow curves matched well, while the duration of systole was, on average, 35 msec longer for MRI. The two characteristic peaks in mitral inflow, representing the early and late filling phases, were clearly seen at both CT and MRI. The MRI measurements showed higher peak flow rates for the mitral inflow compared with the CT flow simulations ($P < .01$). For stroke volume and peak flow rate, there were very strong correlations and good agreement between simulations and measurements ($r = 0.80$, $P < .05$ and $r = 0.98$, $P < .05$, respectively) (see Fig 4 and Table 3). The mean difference in stroke volume and peak flow rate between MRI and CT was 13.11 mL and 3.27 mL/sec, respectively. MRI-based aortic outflow was compared with mitral inflow to assess MRI data quality. Both measurements correlated well ($r = 0.90$, $P < .05$), and the mean difference was −0.89 mL between aortic outflow and mitral inflow.

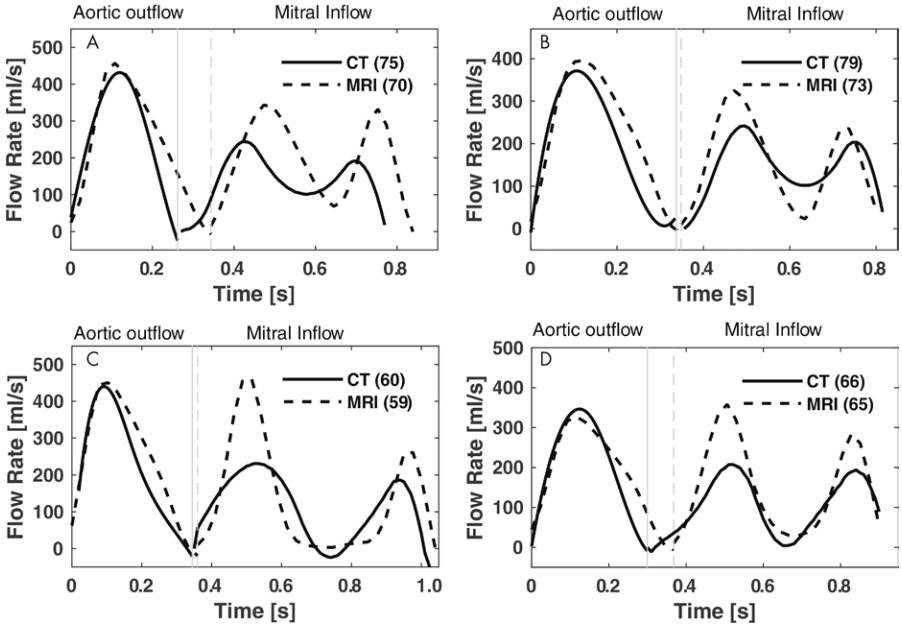

Figure 3: Graphs show flow rates through the aortic valve (during systole) and mitral valve (during diastole) for four of the 12 participants (participants 1–4). The onset of diastole is indicated by a solid line for CT results and a dashed line for MRI results. Heart rates at CT and MRI are indicated by the number in parentheses. (Results for all 12 participants can be found in Figure E3 [online].)

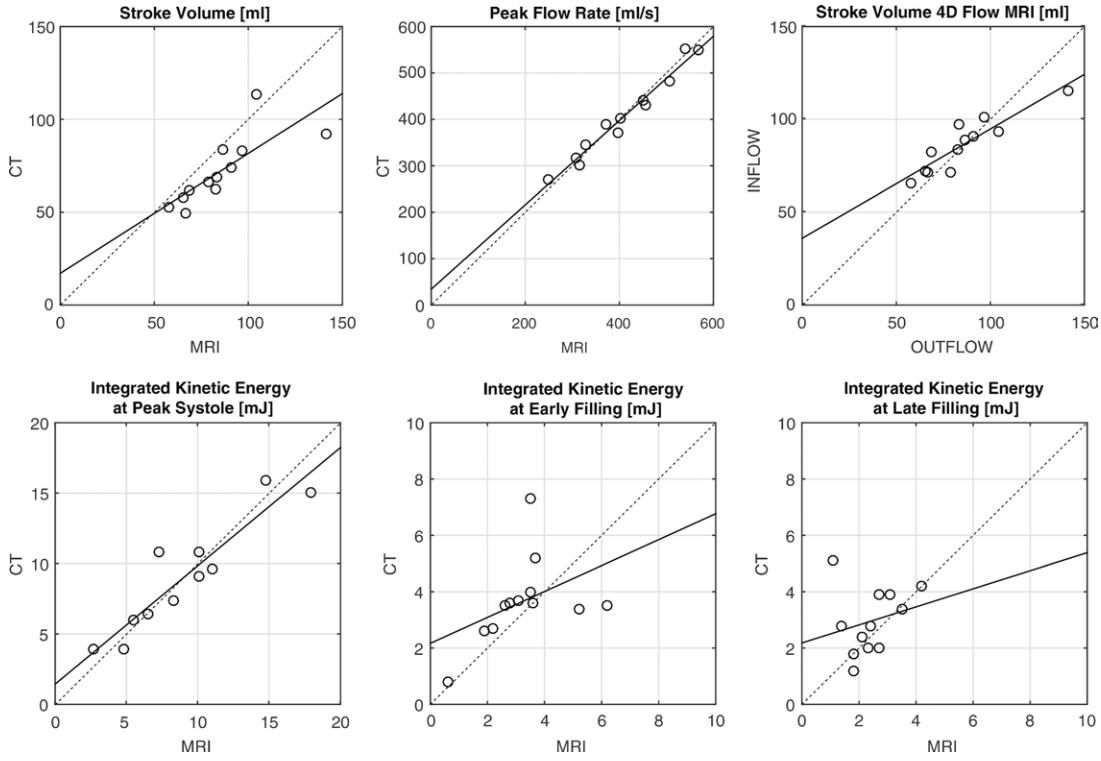

Figure 4: Upper row: Linear regression scatterplots for stroke volume, peak flow rate, and inflow-outflow stroke volumes derived from MRI. Lower row: Linear regression scatterplots for integrated kinetic energy at peak systole, early filling, and late filling. Dotted line = identity line.

Intracardiac Kinetic Energy

The integrated intracardiac kinetic energy was computed and compared for CT and MRI; see Figure 5 for data in the first four participants and Fig E4 (online) for all 12 participants. Three characteristic peaks, representing ventricular emptying and the early and late filling phases, were observed. During early systole, there was a steep increase in kinetic energy as flow accelerated. After peak systole, the flow decelerated and kinetic energy decreased. During the mitral inflow phases, kinetic energy increased again as a result of ventricular relaxation and atrial contraction. The kinetic energy at peak systole showed good correlation and agreement ($r = 0.95$, $P < .05$; mean difference, 0.16 mJ), while at early and late filling, no significant correlations were observed (see Table 3).

Flow Component Analysis

Flow component analyses were performed to assess the flow organization within the LV and to further assess the possibilities of the 4D flow CT technique. Three participants (participants 1, 7, and 8) had an inflow-outflow difference of more than 10%. Data in these participants were not included in the statistical analysis but are included for completeness in Figure 6, marked with an asterisk. Previous studies have shown that the direct flow component decreases in dilated and dysfunctional LVs (17). Comparison between MRI and CT showed low bias (5.1%, −3.47%, −2.56%, and 0.93%) for the four flow components (see Table 3), and the direct flow and residual volume components had a very strong correlation ($r = 0.92$, $P < .05$; mean difference, 5.10% and $r = 0.87$, $P < .05$; mean difference, 0.94%, respectively) while retained inflow and delayed ejection flow did not show any significant correlation because of clustering of data points.

Discussion

In our study, we show that our 4D flow CT method, based entirely on clinically available CT data, can produce both qualitatively and quantitatively similar intracardiac blood flow patterns in a cohort of patients with heart disease, compared with the current reference standard, 4D flow MRI. Because the two techniques are fundamentally different and do not share any measurement data, the results indicate that the 4D flow CT method is able to produce intracardiac flow fields that are similar to in vivo 4D flow MRI measurements.

Of note, information on intracardiac kinetic energy and LV flow components needs to be measured and computed from either 4D flow MRI or 4D flow CT and is not directly measurable from CT or MRI images. Kinetic energy quantifies intracardiac blood flow in a conceptual approach compared with established clinical measures of cardiac function and has been shown to be altered in patients with heart failure compared with healthy subjects (17,18). Hence, intracardiac kinetic energy could potentially be used for heart failure classification (19). Furthermore, in patients with congenital heart diseases such as repaired tetralogy of Fallot and Fontan circulation, kinetic energy levels have the potential to add to the assessment of ventricular dysfunction (20,21). Likewise, flow component analysis could potentially also be used to gain insights into pathophysiology, early diagnosis, treatment options, and prognosis (14,17,22,23). A large residual volume with low or stagnant velocities is expected to

Table 3: Results from Linear Regression Analysis, Where Results from MRI Were Used as the Independent Variable and Results from CT Were Used as the Dependent Variable

Parameter	Slope	*P* Value for Slope	95% Confidence Interval for Slope	Standard Error for Slope	*r* Value	Intercept	*P* Value for Intercept	95% Confidence Interval for Intercept	Standard Error for Intercept	Mean Difference between MRI and CT
Stroke volume (mL)	0.65	.05	0.29, 1.00	0.16	0.80	17.10	.25	−14.35, 48.56	14.12	13.11
Peak flow rate (mL/sec)	0.91	.10	0.79, 1.02	0.050	0.98	34.16	.14	−13.37, 81.69	21.33	3.27
Stroke volume MRI out-in (mL)	0.59	.001	0.39, 0.79	0.09	0.90	35.97	.001	18.26, 53.68	7.95	−0.89
Kinetic energy at peak systole (mJ)	0.84	.08	0.65, 1.03	0.08	0.95	1.44	.16	−0.66, 3.54	0.94	0.16
Kinetic energy at early filling (mJ)	0.46	.10	−0.21, 1.13	0.30	0.44	2.17	.07	−0.19, 4.52	1.06	−0.42
Kinetic energy at late filling (mJ)	0.32	.12	−0.57, 1.21	0.40	0.25	2.18	.06	−0.11, 4.47	1.03	−0.53
Direct flow component (%)	0.86	.34	0.55, 1.18	0.13	0.93	−1.77	.623	−10.01, 6.47	3.49	5.10
Retained flow component (%)	0.34	.04	−0.30, 0.98	0.27	0.43	17.35	.02	3.85, 31.07	5.76	−3.47
Delayed ejection flow component (%)	0.17	.002	−0.24, 0.58	0.17	0.35	20.89	.001	11.69, 30.10	3.89	−2.57
Residual volume flow component (%)	0.91	.66	0.45, 1.37	0.120	0.87	1.944	.78	−13.42, 17.31	6.50	0.94

Note.—*P* values for slope indicate if the slope was significantly different from 1, while *P* values for intercept indicate if the intercept was significantly different from 0.

promote intraventricular thrombus formation (17), and a detailed analysis of flow component levels could potentially detect LV dysfunction in subtle or subclinical LV remodeling (23).

Both imaging techniques were able to produce similar results, but their strengths and weaknesses make them suitable for different applications. Although CT uses ionizing radiation to acquire data, clinical scan protocols now include radiation dose reduction tools that greatly reduce the ionizing dose while retaining image quality. MRI does not involve any radiation, but image quality and spatial resolution are lower compared with those at CT. With CT, submillimeter resolution is attainable, which, unlike MRI, enables the study of the effects of trabeculae and papillary muscles on flow quantifications. Also, 4D flow MRI acquisitions normally span hundreds of consecutive heartbeats, making beat-to-beat variations impossible to study. Therefore, in the majority of diseases with irregular cardiac cycles, it is impossible to quantify blood flow reliably using MRI. Furthermore, patients with metallic implants are often excluded from MRI measurements because the implants often cause image artifacts and may not be suitable for MRI. Conversely, CT acquisition is normally performed within one to three heartbeats. Metallic implants may result in some streaking artifacts from photon starvation, but these are not as detrimental to image quality, making the 4D flow CT method a potentially better choice for such patient groups. However, when a 4D flow MRI acquisition is completed, the flow data are readily available. Although the clinical CT acquisition is fast, the flow modeling procedure is currently time consuming, computationally expensive, and unable to handle valvular regurgitation. Because the 4D flow CT method relies on modeling, "what-if" scenarios might be possible whereby such issues as the optimal positioning for a prosthetic valve are explored. In addition, simulations could complement existing clinical imaging modalities and provide information on such elements as shear stress and forces that are otherwise inaccessible. Clearly, the choice of technique is dependent on the application and the objective of the study.

While many flow parameters were found to be similar for 4D flow CT and 4D flow MRI, stroke volume was consistently lower for 4D flow CT. This could be due to a number of reasons. Even though the CT and MRI acquisitions were performed within 2 hours of each other, small differences in the hemodynamic status of the participant may have been present. The two image modalities also acquire data differently. MRI acquisition is the average of several hundred heartbeats during free breathing, and is performed with a breathing navigator at an end-respiratory position. Following clinical protocol, the CT acquisition is performed over three heartbeats and at a slight inspiration breath hold over 7–10 seconds. During inspiration, the venous return to the right side increases, which decreases LV filling by means of interventricular interaction. In addition, LV stroke volume increases slightly during expiration, and these two mechanisms combined could explain the difference in stroke volume between MRI and CT. Performing the CT acquisition at expiration breath holds would probably minimize physiologic differences. Also, inaccuracies in the MRI measurements, indicated by the observed variations

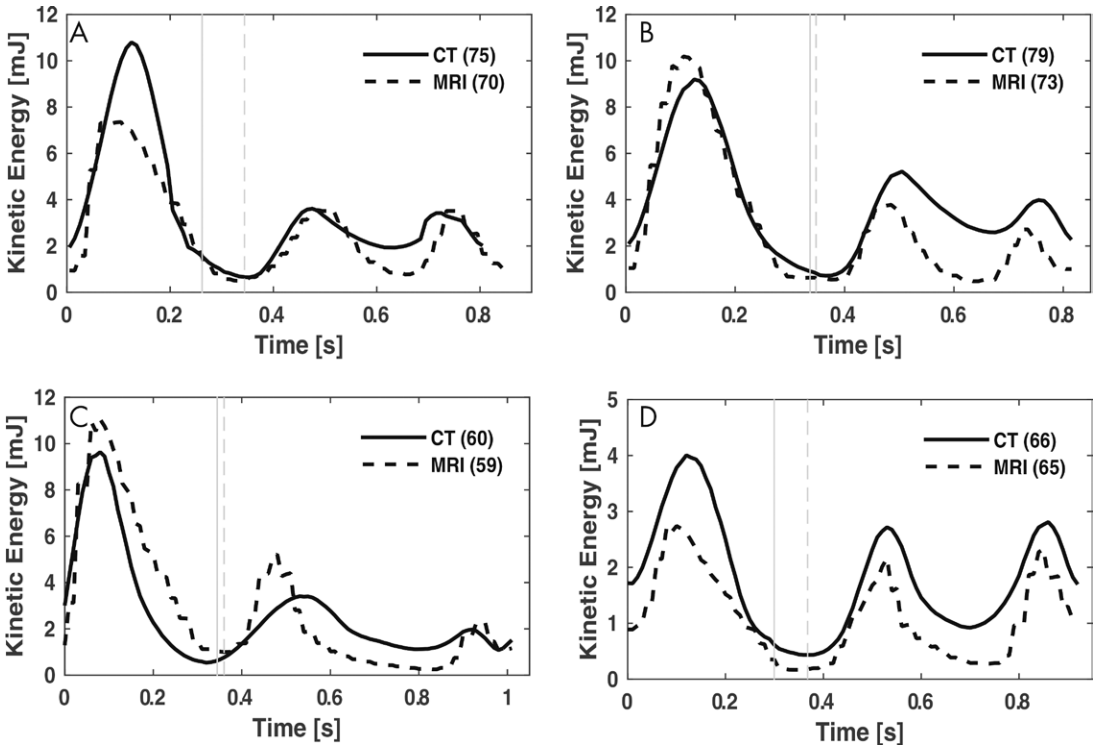

Figure 5: Graphs show integrated intracardiac kinetic energy for four of the 12 participants (participants 1–4). The onset of diastole is indicated by a solid line for CT results and a dashed line for MRI results. Heart rates at CT and MRI are indicated by the number in parentheses. (Results for all 12 participants can be found in Figure E4 [online].)

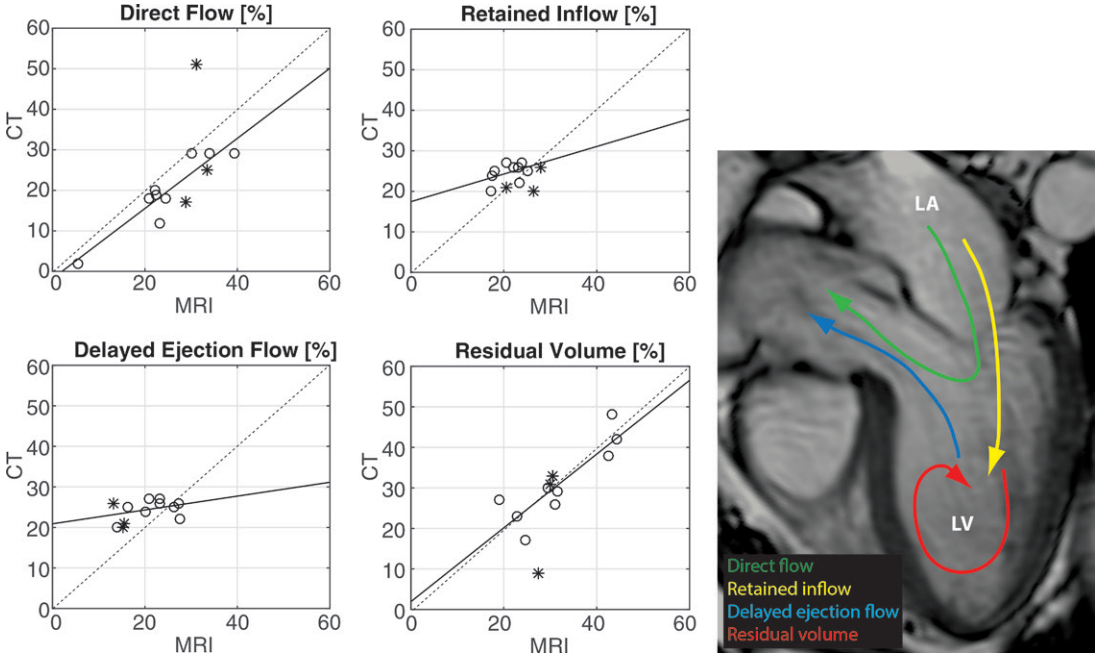

Figure 6: Linear regression scatterplots for the flow component analysis. Dotted line = identity line. Three participants (1, 7, and 8, marked with *) had more than a 10% difference in left ventricular *(LV)* inflow-outflow flow volumes because of suboptimal data artifacts in the MRI data, and the MRI-based flow component analysis was not considered to be reliable. The results for these participants are shown in the figure but were not included in the statistical analysis. The image on the right provides an explanation of the four different flow components in the left ventricle. *LA* = left atrium.

in mitral inflow and aortic outflow, could contribute to the observed differences in stroke volume using simulations and measurement. The inter- and intravariability of flow components derived from 4D flow MRI were recently investigated in a scan-rescan study (24). It was found that results were stable within a population over time and that variations in individuals over time were greater than could be attributed to sources of error in the data acquisition and analysis, suggesting that

additional physiologic factors may influence LV flow measurements. Our method is limited to retrospectively gated CT scans because the motion over the whole cardiac cycle is needed. This will typically increase radiation exposure and could potentially limit the pool of eligible patients. There were no participants in this study with complex cardiac pathologic conditions. A limitation of our study was the relatively small number of participants, and larger prospective studies are required to further establish the diagnostic performance of 4D flow CT compared with MRI.

In closing, a 4D flow CT method based on clinically available CT data produced qualitatively and quantitatively similar intracardiac blood flow patterns compared with the current reference standard, 4D flow MRI, and therefore has the potential to provide incremental value in the assessment of both acquired and congenital heart disease.

Acknowledgments: The authors acknowledge funding from the Knut and Alice Wallenberg Foundation through the project *Seeing Organ Function* and the Swedish Heart Lung Foundation. The simulations were performed on resources provided by the Swedish National Infrastructure for Computing at the National Supercomputer Centre.

Author contributions: Guarantors of integrity of entire study, J.L., V.G., T.E.; study concepts/study design or data acquisition or data analysis/interpretation, all authors; manuscript drafting or manuscript revision for important intellectual content, all authors; approval of final version of submitted manuscript, all authors; agrees to ensure any questions related to the work are appropriately resolved, all authors; literature research, J.L., M.K., A.P., C.J.C.; clinical studies, L.H., A.P.; experimental studies, J.L., V.G., A.P.; statistical analysis, J.L.; and manuscript editing, all authors

Disclosures of Conflicts of Interest: **J.L.** disclosed no relevant relationships. **V.G.** disclosed no relevant relationships. **L.H.** disclosed no relevant relationships. **M.K.** disclosed no relevant relationships. **A.P.** disclosed no relevant relationships. **C.J.C.** disclosed no relevant relationships. **T.E.** disclosed no relevant relationships.

References

1. Sengupta PP, Pedrizetti G, Narula J. Multiplanar visualization of blood flow using echocardiographic particle imaging velocimetry. JACC Cardiovasc Imaging 2012;5(5):566–569.
2. Mittal R, Seo JH, Vedula V, et al. Computational modeling of cardiac hemodynamics: current status and future outlook. J Comput Phys 2016;305:1065–1082.
3. Taylor CA, Fonte TA, Min JK. Computational fluid dynamics applied to cardiac computed tomography for noninvasive quantification of fractional flow reserve: scientific basis. J Am Coll Cardiol 2013;61(22):2233–2241.
4. Zarins CK, Taylor CA, Min JK. Computed fractional flow reserve (FFTCT) derived from coronary CT angiography. J Cardiovasc Transl Res 2013;6(5):708–714.
5. Leipsic J, Yang TH, Thompson A, et al. CT angiography (CTA) and diagnostic performance of noninvasive fractional flow reserve: results from the Determination of Fractional Flow Reserve by Anatomic CTA (DeFACTO) study. AJR Am J Roentgenol 2014;202(5):989–994.
6. Nørgaard BL, Leipsic J, Gaur S, et al. Diagnostic performance of noninvasive fractional flow reserve derived from coronary computed tomography angiography in suspected coronary artery disease: the NXT trial (Analysis of Coronary Blood Flow Using CT Angiography: Next Steps). J Am Coll Cardiol 2014;63(12):1145–1155.
7. Vedula V, Seo JH, Lardo AC, Mittal R. Effect of trabeculae and papillary muscles on the hemodynamics of the left ventricle. Theor Comput Fluid Dyn 2016;30(1-2):3–21.
8. Lantz J, Henriksson L, Persson A, Karlsson M, Ebbers T. Patient-specific simulation of cardiac blood flow from high-resolution computed tomography. J Biomech Eng 2016;138(12):121004.
9. Chnafa C, Mendez S, Nicoud F. Image-based large-eddy simulation in a realistic left heart. Comput Fluids 2014;94:173–187.
10. Mihalef V, Ionasec RI, Sharma P, et al. Patient-specific modelling of whole heart anatomy, dynamics and haemodynamics from four-dimensional cardiac CT images. Interface Focus 2011;1(3):286–296.
11. Bongartz G, Golding SJ, Jurik AG, et al. European guidelines for multislice computed tomography. Luxembourg: European Commission, 2004.
12. Klein S, Staring M, Murphy K, Viergever MA, Pluim JP. elastix: a toolbox for intensity-based medical image registration. IEEE Trans Med Imaging 2010;29(1):196–205.
13. Gupta V, Lantz J, Henriksson L, et al. Automated three-dimensional tracking of the left ventricular myocardium in time-resolved and dose-modulated cardiac CT images using deformable image registration. J Cardiovasc Comput Tomogr 2018;12(2):139–148.
14. Eriksson J, Carlhäll CJ, Dyverfeldt P, Engvall J, Bolger AF, Ebbers T. Semi-automatic quantification of 4D left ventricular blood flow. J Cardiovasc Magn Reson 2010;12(1):9.
15. Carlhäll CJ, Bolger A. Passing strange: flow in the failing ventricle. Circ Heart Fail 2010;3(2):326–331.
16. Fredriksson AG, Zajac J, Eriksson J, et al. 4-D blood flow in the human right ventricle. Am J Physiol Heart Circ Physiol 2011;301(6):H2344–H2350.
17. Eriksson J, Bolger AF, Ebbers T, Carlhäll CJ. Four-dimensional blood flow-specific markers of LV dysfunction in dilated cardiomyopathy. Eur Heart J Cardiovasc Imaging 2013;14(5):417–424.
18. Carlsson M, Heiberg E, Toger J, Arheden H. Quantification of left and right ventricular kinetic energy using four-dimensional intracardiac magnetic resonance imaging flow measurements. Am J Physiol Heart Circ Physiol 2012;302(4):H893–H900.
19. Kanski M, Arvidsson PM, Töger J, et al. Left ventricular fluid kinetic energy time curves in heart failure from cardiovascular magnetic resonance 4D flow data. J Cardiovasc Magn Reson 2015;17(1):111.
20. Jeong D, Anagnostopoulos PV, Roldan-Alzate A, et al. Ventricular kinetic energy may provide a novel noninvasive way to assess ventricular performance in patients with repaired tetralogy of Fallot. J Thorac Cardiovasc Surg 2015;149(5):1339–1347.
21. Sjöberg P, Heiberg E, Wingren P, et al. decreased diastolic ventricular kinetic energy in young patients with Fontan circulation demonstrated by four-dimensional cardiac magnetic resonance imaging. Pediatr Cardiol 2017;38(4):669–680 [Published correction appears in Pediatr Cardiol 2017;38(5):1087.].
22. Dyverfeldt P, Bissell M, Barker AJ, et al. 4D flow cardiovascular magnetic resonance consensus statement. J Cardiovasc Magn Reson 2015;17(1):72.
23. Svalbring E, Fredriksson A, Eriksson J, et al. Altered diastolic flow patterns and kinetic energy in subtle left ventricular remodeling and dysfunction detected by 4D Flow MRI. PLoS One 2016;11(8):e0161391.
24. Stoll VM, Loudon M, Eriksson J, et al. Test-retest variability of left ventricular 4D flow cardiovascular magnetic resonance measurements in healthy subjects. J Cardiovasc Magn Reson 2018;20(1):15.